Renewable Energy 193 (2022) 1049–1061

Contents lists available at ScienceDirect

Renewable Energy

journal homepage: www.elsevier.com/locate/renene

An experimental investigation of a roof-mounted horizontal-axis wind turbine in an idealized urban environment

Arslan Salim Dar [a], Guillem Armengol Barcos [a, b], Fernando Porté-Agel [a, *]

[a] Wind Engineering and Renewable Energy Laboratory (WIRE), École Polytechnique Fédérale de Lausanne (EPFL), 1015, Lausanne, Switzerland
[b] Escola Tècnica Superior d'Enginyeria Industrial de Barcelona (ETSEIB), Universitat Politècnica de Catalunya (UPC), 08028, Barcelona, Spain

ARTICLE INFO

Article history:
Received 16 February 2022
Received in revised form
30 March 2022
Accepted 6 May 2022
Available online 16 May 2022

Keywords:
Urban environment
Wind energy
Buildings
Power performance
Wakes

ABSTRACT

Wind-tunnel experiments are performed to investigate the effect of minor modifications to the roof edge shape on the power performance and wake characteristics of a horizontal-axis wind turbine sited on a cube-shaped building. Three roof edge shapes are considered: a sharp edge, a rounded edge, and a solid fence. The power performance of the turbine is dependent on its streamwise position, and on the roof edge shape due to the difference in the flow shear induced by different roof edges. The sharp edge and solid fence cases show high variation in power with the turbine position, which is reduced significantly in the rounded-edge case. The turbine shows the worst power performance regardless of its position in the fence case. The roof edge shape is also found to affect the wind turbine wake. Specifically, the wake recovery and expansion rates are found to be greatest for the fence case, and they decrease with the increasing smoothness of the roof edges. This is related to the difference in the base flow turbulence induced by different roof edge shapes. Compared to the base flow, turbulence intensity in the wake is reduced on the building, except at the rotor top tip level.

1. Introduction

Our world has undergone intense urbanization, with the global population living in urban areas increasing from 30% in 1950 to 55% in 2016 [1,2]. In the developed world, these numbers are even higher, with more than 80% of the population living in urban areas [2]. This rapid urbanization has also resulted in an overall increase in the global energy demands. Although most of the world energy needs are currently provided by fossil fuels; renewable energy sources have emerged as a promising alternative to decarbonize the energy market, and potentially mitigate the harmful impact of fossil fuels on the environment. In this context, it is also relevant to highlight the sustainable development goals (SDGs) promoted by the United Nations [3], two of which concern the promotion of renewable energy sources and the development of sustainable cities. Localized micro-generation of energy within urban environments via renewable sources can play a crucial role in achieving the above-mentioned SDGs. While wind energy is traditionally harvested from wind farms sited away from urban settlements, wind energy generation within the urban environment has been highlighted as an under-explored potential for clean energy generation closer to the end consumer [4].

Several studies have explored the potential and challenges associated with urban wind energy. Stathopoulos et al. [5] reviewed recent developments in the field of urban wind energy. They stressed on the need to further explore the influence of building aerodynamics on the potential wind energy generation and wind resource assessment. Micallef and van Bussel [6] also presented a review of urban wind energy research with a special focus on urban aerodynamics. They highlighted that urban wind energy research suffers from a lack of synergistic efforts between different areas of research, which is crucial for the success of urban wind energy. Walker [7] reviewed the methods used for urban wind resource assessment, and showed that the most common approach of combining a wind turbine power curve with the wind rose information gives inaccurate estimation of potential urban wind energy yield. This was associated with the complexity of flow in an urban environment including the influence of the shape of the buildings. Concerns regarding the noise generation and public acceptance of urban wind energy also present a challenge [6,8]. Despite these challenges, the assessment of urban wind energy on a national or regional scale shows that it can play a significant role in providing

* Corresponding author.
E-mail addresses: arslan.dar@epfl.ch (A.S. Dar), fernando.porte-agel@epfl.ch (F. Porté-Agel).

https://doi.org/10.1016/j.renene.2022.05.035

decentralized renewable energy. Mithraratne [9] performed an assessment of urban wind energy generation using roof-mounted wind turbines in New Zealand. They showed that, while urban wind energy cannot act as an alternative for the large-scale wind energy generation, it has the potential to reduce the carbon footprint of New Zealand's electricity generation. Drew et al. [10] assessed the potential of wind energy generation within the Greater London area in the UK. They found that most areas with high wind energy potential were located towards the outskirts of the city, although some areas closer to the city center also had high potential for wind energy generation. Grieser et al. [11] studied the economic feasibility of small wind turbines in urban environments in Germany. They showed that optimized positioning of wind turbines in an urban environment based on flow conditions is crucial. In addition, combining a wind energy generation system with an energy storage system was observed to enhance the economic feasibility of urban wind energy generation. More recently, Rezaeiha et al. [4] developed a framework to assess wind energy potential of roof-mounted wind turbines. When applied to the Netherlands, they found that across existing high rise buildings in 12 cities of the Netherlands, an annual energy production of 150.1 GWh can be achieved.

Assessment of wind resources in an urban environment is, however, a challenging task due to the complex nature of urban flow and its strong dependence on building aerodynamics. Different studies have been reported in the literature that assess the potential energy yield of wind turbines in an urban environment. Bayoumi et al. [12] developed a tool to optimize the integration of a vertical axis wind turbine in the building design in order to achieve a certain energy yield. Their model relied on some pre-computed computational fluid dynamics results of flow around the buildings, and was able to provide an estimation of the optimal number, position and size of the turbines required to generate the target energy yield. Abohela et al. [13] investigated the effect of wind direction, turbine position and roof shapes (such as flat, dome-shaped, pyramid-shaped and vaulted) on the energy yield of wind turbines. They concluded that an informed decision based on the understanding of flow around the building and optimal placement of wind turbines can result in an increase in the potential energy yield. Al-Quraan et al. [14] compared wind tunnel measurements of flow around buildings with field data to assess the accuracy of wind tunnel measurements. They concluded that, while wind tunnel data showed good agreement with the field data for an initial assessment of wind energy potential, the agreement between the two decreased with the increase in the inhomogeneity of the surrounding terrain. Emejeamara et al. [15] proposed a new method for estimating power production of vertical axis wind turbines, which could also account for unsteady power performance of the turbine due to turbulent nature of the flow. Rezaeiha et al. [4] developed a framework to assess the wind energy potential using the information of building aerodynamics, wind speed at building height, turbine characteristics and number of turbines. They demonstrated the use of the framework by computing the annual energy production using roof-mounted turbines across the Netherlands. Ruiz et al. [16] presented an optimization of ducted openings in high rise buildings for wind energy harvesting. They optimized the design of the ducted opening by changing the fillet radius and diameter of the duct, and showed that aerodynamic design of the buildings can significantly enhance wind energy production. Li et al. [17] showed that an array of vertical axis turbines optimized for the roof shape can lead to enhanced power performance. More recently, Higgins and Stathopoulos [18] took an artificial intelligence (AI) approach to assess the potential of urban wind energy. They developed artificial neural network (ANN) and tested its performance for different city configurations against wind tunnel data. They concluded that AI modeling can prove to be a useful tool for identification and assessment of potential turbine locations in an urban environment.

While the potential of urban wind energy has been readily reported in the literature, the interaction of wind turbines with the atmospheric boundary layer in an urban environment is relatively under-explored. For the large-scale wind energy, this has been the focus of research over the past few decades [19,20]. The general working principles of horizontal axis wind turbines, their aerodynamics and momentum theory are covered in detail in Refs. [21,22]. The wake of a turbine, characterized by its low velocity and turbulent nature, is responsible for reduction in power available for downstream turbines. Accounting for the turbine wake effects is, therefore, important for clustering of wind turbines in an urban environment. In addition, these wakes can also alter the fatigue load distribution on downstream turbines, as well as on any built structures downstream of the turbine. It is, therefore, of great interest to understand how turbine wakes evolve in urban environments. Due to their potential impact on the success of any wind energy project, several studies investigating wind turbine wakes in an urban environment have recently emerged. Ge et al. [23] investigated the effect of the wake of a turbine on an urban district model located downstream, where the turbine hub height and diameter were twice the height of the buildings. They found that the urban district resulted in a faster recovery of the turbine wake and modified its trajectory. The turbine wake also reduced the wind speed in the streamwise streets of the urban district. Ge et al. [24] also performed large-eddy simulation of single and multiple wind turbines located downstream of a cube-shaped building. They showed that the building resulted in a decrease in power and increase in power fluctuations of the first turbine located downstream. The turbine wake also showed faster recovery due to higher turbulence and secondary mean flow induced by the building. A second turbine placed downstream of the first one showed higher power output in the presence of the building than in its absence. Fan et al. [25] studied the effect of buildings and trees on the performance of roof-mounted wind turbines. Their results showed that trees higher than buildings caused a decrease in the power output of the turbines compared to the case with trees lower than the building height. The wake of the turbine was asymmetric and had a downward trajectory. Xu et al. studied vertical axis wind turbines located on the side of [26], and between [27] buildings. For wind turbines on the side of the buildings, different flow scenarios and arrangements of turbines were simulated. From these simulations, they deduced that for a stand-alone turbine, tailwind position performed best, whereas for multiple turbines a combination of crosswind and tailwind arrangement proved best. For wind turbines installed between the buildings, counter-rotating turbine arrangement performed better than the co-rotating arrangement. They also placed five arrays of wind turbines between the buildings, and showed that their performance was rather complex and dependent on the flow conditions. The effect of wind direction was also investigated, revealing best performance at 15° incoming wind direction. All of the above-mentioned studies utilize numerical tools, and there is an obvious lack of experimental work investigating the interaction of wind turbines with an urban environment.

Urban wind energy can also benefit from recent advances in the field of wind energy in complex terrain. Several studies have shown that local changes in terrain elevation can have significant effects on wind resources available for wind turbines [28,29]. In addition, atmospheric stability has also been shown to have significant effect on available power for wind turbines in complex terrain, with higher spatial variability during stable conditions [30]. Especially, the studies focused on wind turbines located on escarpments can be relevant for urban wind energy, as an escarpment can be

considered as a building with infinite length and width. Lange et al. [31] showed that the edge of the escarpment can have a significant effect on the flow over it, and consequently on the power available for turbines. Qian & Ishihara [32] showed that the ratio of escarpment height to the turbine height can have an effect on the turbine wake deflection. More recently, Dar & Porté-Agel [33,34] showed that the shape of the escarpment leading-edge significantly affects the wake of a wind turbine sited on it.

In the current study, we have performed wind tunnel measurements on a roof-mounted wind turbine in an idealized urban environment, where the building is represented by a cube-shaped block. Of particular interest is the shape of the roof edges, where minor modifications, such as slight curvature or addition of a boundary fence, are introduced in addition to a sharp-edged roof. The sensitivity of the turbine power output to the roof edge shape and streamwise position of the turbine on the building is first investigated. The wake of the turbine placed at the position corresponding to maximum power output is then compared between different roof edge shapes. To the best of the authors' knowledge, this is the first wind tunnel study investigating the effect of seemingly minor modifications of the roof edge shapes and turbine position on the power performance and wake characteristics of a roof-mounted wind turbine. The rest of the article is structured as follows: section 2 documents the experimental setup and the urban boundary layer developed; results from the study are reported and discussed in section 3; finally, a summary of the work and conclusions are presented in section 4.

2. Experimental setup

The experiments are conducted in the closed-loop boundary layer wind tunnel at the WiRE laboratory of EPFL. The wind tunnel has a test section of 28 m length, 2.6 m width and 2 m height, with a contraction of 5:1 area ratio before the inlet. A 130 kW fan drives the flow in the wind tunnel.

A miniature three-bladed horizontal axis wind turbine is used in this study. The miniature turbine is a scaled-down version of the WiRE-01 miniature turbine developed at WiRE, EPFL [35,36]. A scaling ratio of 1:1.43 is established between the scaled-down and original turbine models. This scaling results in a rotor diameter d of 10.5 cm and a hub height z_h of 8.75 cm for the scaled-down turbine. The blade profile has a circular arc shape with a sharp leading-edge, where the chord length varies from 8.4 mm at the blade root to 5.88 mm at the tip. The rotor is built from a liquid photopolymer resin by 3D printing. The rotor is mounted on a direct current (DC) motor manufactured by Maxon motors (model: DCX10L), which has a diameter of 10 mm (leading to a rotor to nacelle diameter ratio of 10.5) and length of 25 mm. The DC motor is controlled by a servo controller (model: ESCON 36/2 DC) via a digital encoder (model: ENX10).

The performance of the scaled-down turbine is first characterized and compared with the original turbine model. For this purpose, power and thrust measurements are made in a flat terrain. The power produced by the turbine P is measured by multiplying the shaft torque Q with the rotational speed Ω of the turbine. For more details on power measurements procedure, the reader is referred to Ref. [35]. The power coefficient C_p is then calculated by the following relation:

$$C_p = \frac{P}{\frac{1}{2}\rho A \bar{u}_h^3} = \frac{Q\Omega}{\frac{1}{2}\rho A \bar{u}_h^3}, \tag{1}$$

where ρ is the air density, A is the rotor swept area and $\bar{u}_h$ is the mean streamwise velocity at the hub height. In order to measure the thrust force T, the turbine is mounted on a multi-axis strain gauge sensor (model: ATI-nano-17Ti). Similar to the power coefficient, the thrust coefficient C_T is calculated by:

$$C_T = \frac{T}{\frac{1}{2}\rho A \bar{u}_h^2}, \tag{2}$$

where T is the total thrust force measured by the strain gauge sensor. The averaged streamwise velocity at the hub height $\bar{u}_h$ (measured by a pitot static tube) is kept at 6.7 ms^{-1} for these measurements. The velocity $\bar{u}_h$ is chosen to establish a dynamic similarity in terms of the Reynolds number Re_d (based on $\bar{u}_h$ and rotor diameter d) between the original and scaled-down turbine models. For the original WiRE-01 turbine, the power and thrust coefficient data is obtained from Ref. [37], which has approximately the same Re_d (~ 47000) as in the current experiments. Fig. 1 shows the comparison of the power and thrust coefficients as a function of tip speed ratio λ between the scale-down and original turbine models. Here, it should be noted that the tip speed ratio is varied by varying the rotational speed of the turbine, while keeping the incoming velocity constant. Both turbines show very similar trends and values of the power and thrust coefficients. The maximum power coefficient is 0.34 and 0.35 for the scaled-down and original turbines, respectively, at a tip speed ratio of around 3.8. The thrust coefficient at λ corresponding to maximum C_p is about 0.8 and 0.82 for the scaled-down and original turbine models, respectively. This comparison shows that scaling down the turbine does not affect its performance characteristics. For subsequent measurements in the

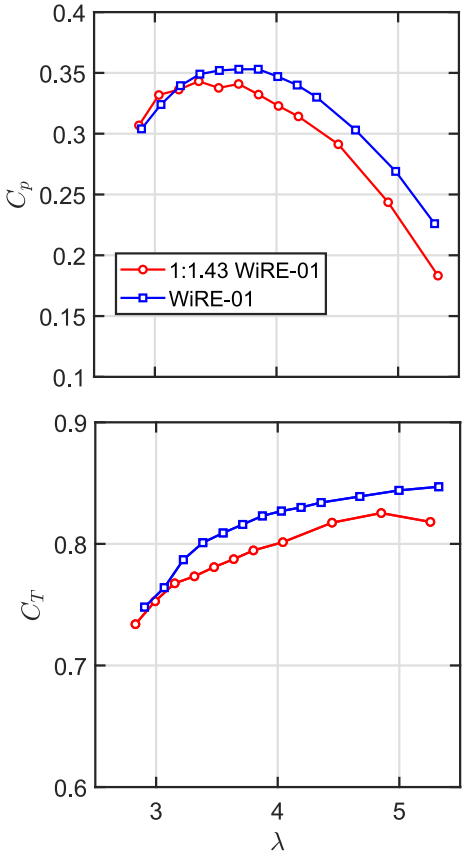

Fig. 1. Comparison of the power (top) and thrust (bottom) coefficients as a function of tip speed ratio between the original and scaled-down turbine models.

urban boundary layer, the turbine is operated at the λ corresponding to maximum C_p for each case.

A two-component frequency-shifted laser Doppler velocimetry (LDV) system developed by TSI is used to measure the streamwise and vertical velocity components in the flow. The LDV probe containing the transmitter and receiver optics is mounted on a 3 degrees-of-freedom (DOF) traversing system outside the test section of the wind tunnel. In order to increase the focal length of the transmitter, a beam expander is fitted in front of the LDV probe. The total focal length of the LDV transmitter is 2.29 m. The flow is seeded with olive oil droplets, which have a diameter on the order of several micrometers. Flow seeding is done through a slot in the tunnel floor at the inlet of the test section. This ensures that the seeding method does not influence the flow in the test section, especially, around the building. Data is acquired using the FlowSizer-64 software (also developed by TSI). The velocity statistics are weighted by the transit time (also known as the gate time) of the tracer particles to compensate for high velocity bias, which occurs because the particles with higher velocity travel further and, thus, have a higher probability of getting sampled.

An idealized urban canopy model is set up inside the test section to simulate an urban boundary layer. The idea is to have a relatively taller building surrounded by a set of smaller ones. The small buildings are represented by square base prisms, with the base dimensions of 8 cm $\times$ 8 cm and height of 10 cm. The square base prisms are arranged in a staggered configuration, with a spanwise and streamwise spacing of two and four times their length, respectively. Similar arrangements have been used in the past to investigate flows within and above urban canopies. Castro et al. [38] performed wind tunnel measurements using a staggered configuration of cubic blocks to understand urban boundary layer flows. Similarly, Cheng and Porté-Agel [39] compared the staggered and aligned configurations of cubic arrays using large-eddy simulation to investigate the adjustment of boundary layer to urban surfaces. A picket fence of 2.5 m in width with a total height of 13 cm, including saw-tooth shaped spikes of width and height equal to 3 cm, is also placed at the inlet of the test section to enhance turbulence production.

The taller buildings used for mounting a turbine are cube-shaped, with a height of 40 cm. This yields a ratio of 4 between the height of the tall building and surrounding urban canopy. The ratio between the building height and turbine hub height is 4.5, showing that the turbine is considerably smaller than the building it is placed on. Minor modifications to the roof edges inspired from roof shapes found in reality are made. Three different roof edge shapes are used, which are described in detail below:

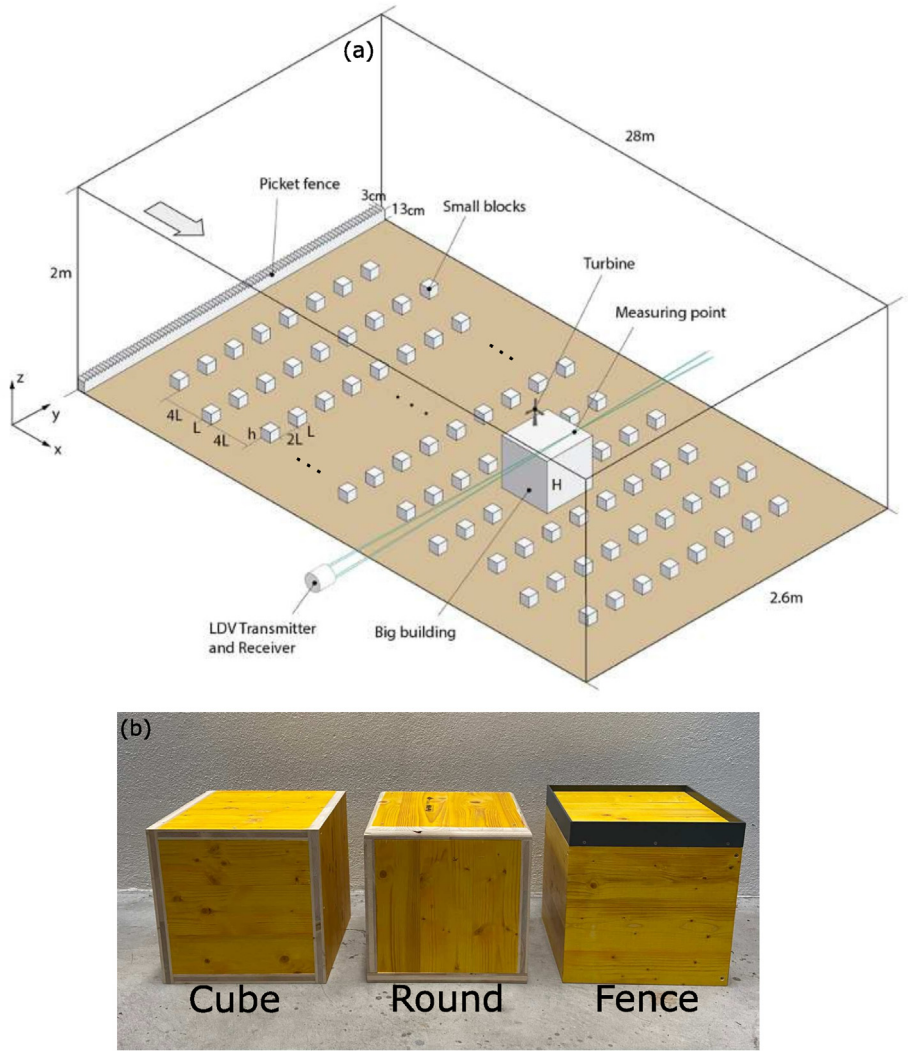

Fig. 2. (a) Sketch of the experimental setup inside the test section; $L = 8$ cm, $h = 10$ cm and $H = 40$ cm. (b) A picture of the cubic tall buildings with modified roof edges.

1. Roof with sharp 90° edges (labeled: Cube).
2. Roof with a curved edge shape, where radius of curvature is 5% with respect to the building height (labeled: Round).
3. Roof with a solid boundary fence, where fence height is also 5% with respect to the building height (labeled: Fence).

A schematic representation of the experimental setup, along with a picture of the cubic buildings used for mounting the turbine, is shown in Fig. 2.

Measurements can be sub-divided into two parts: power measurements and velocity measurements. All measurements are performed with the turbine placed in the center of the building span. For power measurements, the turbine is placed at different streamwise locations to investigate the effect of its distance from the building leading edge on power performance. Once the streamwise position corresponding to maximum power is identified, that position is chosen to place the turbine for velocity measurements, which are carried out with and without the turbine. In the vertical direction, measurements are taken with a spatial resolution of 1 cm, which yields 10 points across the rotor. Above the building, measurements are taken until a height of $2d$; whereas behind the building, measurements are taken from $1d$ below the building height to $2d$ above it. This results in 21 and 33 measurement points in each vertical profile on and behind the building, respectively. Vertical profiles of mean and turbulence quantities at several representative streamwise locations are measured (8 in the base flow and 6 in the wake flow). In total, 204 measurements points for the base flow, and 162 measurement points for the wake flow are considered in each case, where 15000 instantaneous velocity samples are taken at each measurement point to ensure statistical convergence.

The turbulent boundary layer 1 m upstream of the cubic tall building is measured using LDV with a spatial resolution of 2 cm. Fig. 3 shows the vertical profiles of the normalized averaged streamwise velocity, streamwise turbulence intensity and normalized averaged vertical momentum flux. In this figure, $z/d = 0$ represents the test section floor; whereas in the rest of the article, it represents the building roof. The streamwise velocity at the projected height of the turbine center on the building $z_{h,up} = 48.75$ cm in the upstream flow $\bar{u}_{h,up} = 6\ ms^{-1}$ is used for normalization in Fig. 3. The normalized averaged streamwise velocity shows higher shear close to the surface and increases with height. A power law fit according to $\bar{u} = \bar{u}_{h,up}(\frac{z}{z_{h,up}})^n$ is also shown with a blue line in Fig. 3 (a). The shear exponent n of the power law fit is 0.26, which indicates high shear in the flow. The velocity at the maximum height of the boundary layer is 7.29 ms^{-1}. Due to the limitation of optical access, measurements above this height (i.e. 90.5 cm from the test section floor) cannot be taken. Therefore, the boundary layer height is assumed to be equal to 90.5 cm. This assumption is reasonable since the velocity only increases by 1.5% between $z/d = 8$ and $z/d = 8.6$. It is important to note that the boundary layer height is more than twice the height of the cubic building, which means that both the turbine and the building are fully immersed in the boundary layer. Considering that a logarithmic layer constitutes the lowest 10–15% of the boundary layer height, a logarithmic fit is done on the lowest 12.5% of the boundary layer. Following [40], the logarithmic fit is done using the following relation:

$$\bar{u} = \frac{u_*}{\kappa} ln\left(\frac{z - d_0}{z_0}\right), \tag{3}$$

where u_* is the friction velocity, κ is the von Karman constant taken as 0.41, z_0 is the aerodynamic roughness length, and d_0 is the displacement height. The displacement height is implemented to account for the effect of the urban canopy height on the development of the boundary layer. The normalized averaged streamwise velocity together with the logarithmic fit is shown in Fig. 3 (d). The values of friction velocity u_*, aerodynamic roughness length z_0, and displacement height d_0 obtained from the logarithmic fit are 0.41 ms^{-1}, 0.2 cm, and 8.34 cm, respectively. The streamwise turbulence intensity is around 0.2 at the bottom of the boundary layer and decreases almost linearly with height. The decrease in streamwise turbulence intensity with height is related to the decrease in the mean flow shear with height. At the projected height of the turbine center on the building, the streamwise turbulence intensity is 0.12 in the upstream boundary layer. The normalized averaged vertical momentum flux also shows highest values closer to the surface, due to high shear in the flow. Table 1 summarizes key flow parameters in the upstream boundary layer.

3. Results

3.1. Base flow

We first investigate the flow development across the mid span of the building without the turbine, termed as the base flow. Fig. 4

Table 1
Key flow parameters in the upstream boundary layer.

$\bar{u}_{h,up}$ (ms^{-1})	$\bar{u}_\infty$ (ms^{-1})	n	$u_*(ms^{-1})$	$z_o(cm)$	$d_0(cm)$	$\delta(cm)$
6	7.29	0.26	0.41	0.2	8.34	90.5

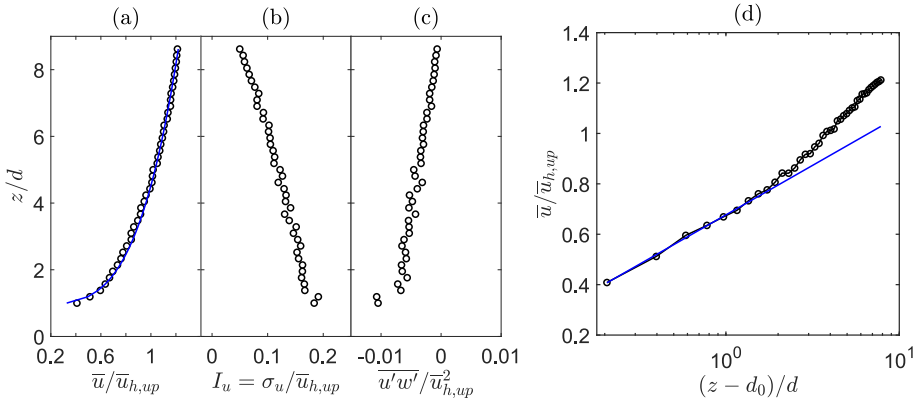

Fig. 3. Vertical profiles of the normalized averaged streamwise velocity with power law fit in blue line (a), streamwise turbulence intensity (b) and normalized averaged vertical momentum flux (c). The normalized averaged streamwise velocity is also plotted in a semi-logarithmic scale with a logarithmic law fit in blue color (d).

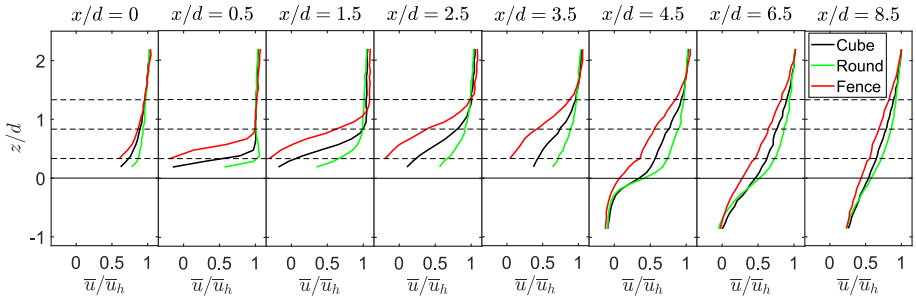

Fig. 4. Vertical profiles of the normalized averaged streamwise velocity in the base flow across the building. The horizontal black solid line traces the height of the building, whereas the black dashed lines trace the prospective rotor bottom tip, hub and top tip locations.

shows a comparison of the vertical profiles of the normalized averaged streamwise velocity in the base flow for different roof edge shapes. For the building with sharp 90° edges (named as 'Cube'), a region of high shear and reverse flow is observed near the building leading edge, close to the surface. With the increase in the streamwise distance, the flow velocity close to the surface increases, along with the height of the high shear region. This is related to the growth of the shear layer that develops across the building roof due to the interaction of the separated flow closer to the surface and the free flow away from the surface. Immediately behind the building at $x/d = 4.5$, there is a sharp transition between the flow under the building height and that above it. This is due to the wake of the building, which has not mixed with the flow above at the given streamwise location. With the increase in the streamwise distance, the building wake grows and mixes with the flow above it, leading to a smoother velocity profile.

For the curved roof shape (named as 'Round'), rounding the roof edges leads to higher velocity and lesser shear across the building roof compared to the Cube case. This is because rounding the roof edges leads to a reduction in the adverse pressure gradient induced by the building, and no flow separation is observed in this case. Behind the building, an even stronger transition between the flow under the building height and that above it is observed compared to the Cube case.

The addition of the solid boundary fence ('Fence' case) results in a stronger separation, with the position of maximum shear located higher than that for the Cube case, which is likely caused by the blockage induced by the boundary fence. Across the building, the Fence case shows highest shear and lowest velocity compared to the rest of the cases. Behind the building, the Fence case also shows highest shear and lowest velocity compared to the other cases, where the differences between different cases reduce with the increase in the downstream distance. It is to be noted that, from here on, $x/d = 0$ represents the building leading edge and $z/d = 0$ represents the building roof surface. The averaged hub height streamwise velocity at the turbine position on the building $\overline{u}_h$ in each respective case is used to normalize all the flow quantities. The choice of the turbine position on the building will be discussed later in section 3.2. The normalization velocity $\overline{u}_h$ is 6.5 ms^{-1}, 6.54 ms^{-1} and 6.38 ms^{-1} for Cube, Round and Fence cases, respectively.

Fig. 5 shows the development of the normalized averaged vertical velocity for the three cases. As can be seen, high vertical velocity values are observed close to the building leading edge. As expected, the Fence case shows highest vertical velocity, with the values decreasing gradually for the Cube and Round cases. For streamwise positions $x/d \geq 2.5$, the vertical velocity is very close to zero above the building height for all cases. Below the building height, positive and negative velocities are observed at $x/d = 4.5$ and $x/d = 6.5$, respectively. This can be related to the flow recirculation that develops behind the building. A turbine would experience high vertical velocity across the rotor if it is located close to the leading edge of the building, and the vertical velocity magnitude would be highest in the Fence case and lowest in the Round case.

In order to characterize the evolution of turbulence across the building, we compute the streamwise turbulence intensity $I_u = \frac{\sigma_u}{\overline{u}_h}$, where σ_u is the standard deviation of the streamwise velocity. Fig. 6 shows a comparison of the streamwise turbulence intensity between the three building cases. High streamwise turbulence intensity values are observed for all cases, where values close to 0.1 are observed in the free stream flow for all cases. The streamwise turbulence intensity is highest in the shear layer developed from the roof leading edge. Peak streamwise turbulence intensity values of around 0.45 are observed for the Fence case at $x/d = 1.5$, 2.5, and for the Cube case at $x/d = 1.5$. The streamwise turbulence intensity showed highest values and stronger variation in the vertical direction for the Fence case, and lowest values for the Round case, with the Cube case showing values somewhere in between. The trends observed in the evolution of streamwise turbulence

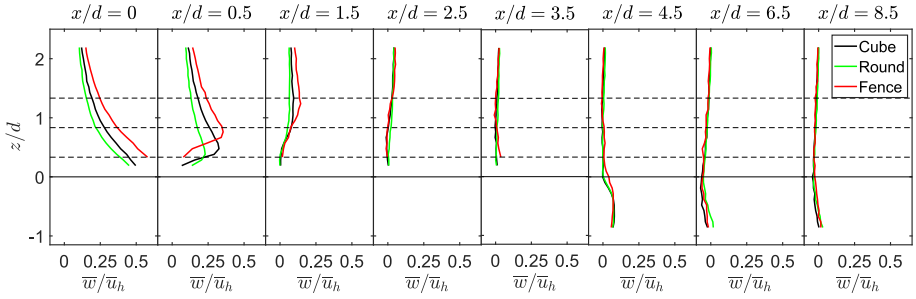

Fig. 5. Vertical profiles of the normalized averaged vertical velocity in the base flow across the building. The horizontal black solid line traces the height of the building, whereas the black dashed lines trace the prospective rotor bottom tip, hub and top tip locations.

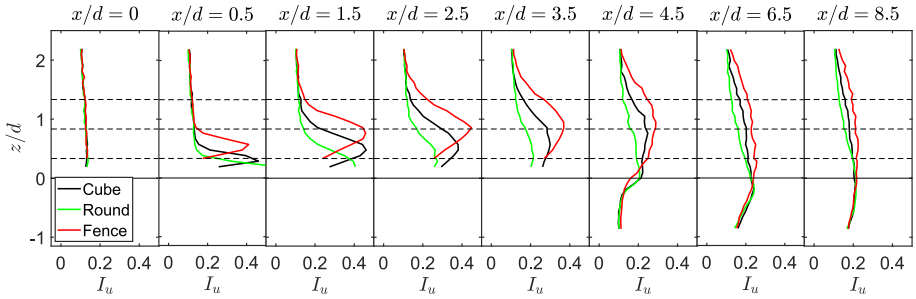

Fig. 6. Vertical profiles of the streamwise turbulence intensity in the base flow across the building. The horizontal black solid line traces the height of the building, whereas the black dashed lines trace the prospective rotor bottom tip, hub and top tip locations.

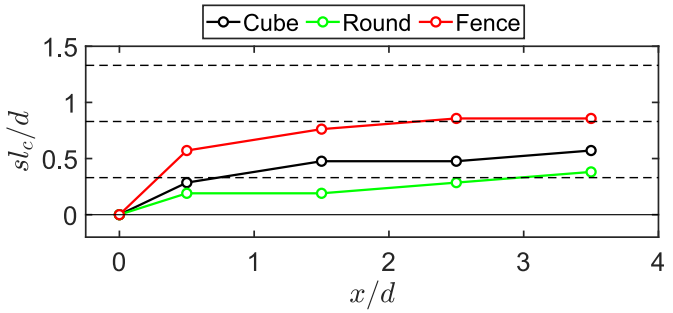

Fig. 7. Growth of the shear layer center as a function of downstream distance. The horizontal black solid line traces the height of the building, whereas the black dashed lines trace the prospective rotor bottom tip, hub and top tip locations.

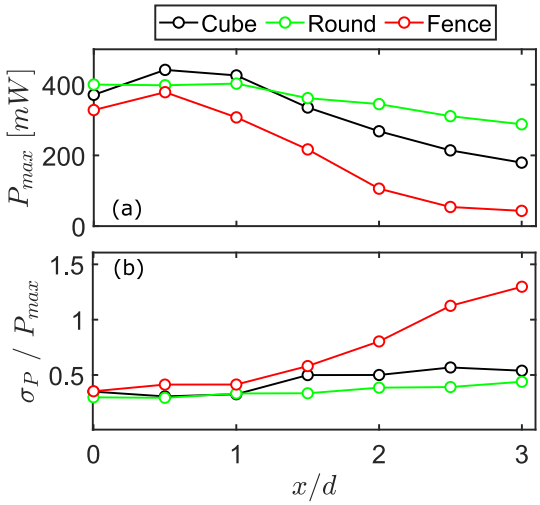

Fig. 8. (a) Maximum mean power produced by the turbine and (b) normalized standard deviation in power as a function of streamwise distance.

intensity are consistent with the shear observed in the mean flow, as higher shear in the Fence case would lead to higher turbulence production compared to the other cases.

The vertical position of the maximum streamwise turbulence intensity also changes with the roof shape. Following Kiya and Sasaki [41], the peak location of the streamwise turbulence intensity can be used to characterize the center of the shear layer that grows from the building roof edge. Fig. 7 shows the growth of the shear layer center for different roof shapes. The shear layer center initially moves vertically up with streamwise distance from the leading edge, but reaches an almost constant value for each case, which is consistent with the observations of Kiya and Sasaki [41]. The center of the shear layer is observed to be highest for the Fence case, coinciding with the turbine hub height at $x/d > 1.5$. For the Round case, it is below the turbine bottom tip height for all locations, except the last one; whereas it is slightly above the bottom tip height for the Cube case. The vertical position of the shear layer center with respect to the rotor is important, as it determines the turbulence profile experienced by the turbine and can have an effect on the fatigue loads on the rotor.

3.2. Power performance

We now focus on the power extracted by the turbine from the base flow. More specifically, we want to understand how the power production is affected by the turbine position on the building, as well as by the roof edge shape. For this purpose, we first plot the maximum mean power produced by the turbine at different streamwise positions for the three cases in Fig. 8(a). The Cube case shows highest power production among all cases at a streamwise position of $x/d = 0.5$, with the maximum mean power dropping for $x/d > 0.5$, where values less than half compared to the peak are observed at $x/d \geq 2.5$. Adding a solid boundary fence leads to not only a decrease in the maximum mean power, but also to a higher variability in the maximum mean power with the streamwise position. Mean power values of approximately 10% compared to the peak value are observed at $x/d \geq 2.5$. Rounding the roof edges leads to a slightly lower peak value compared to the Cube case at $x/d = 0.5$, but it shows the least amount of variation in power with the streamwise position among all the cases. As the wind direction can change in the real world, the variation in mean power production with streamwise distance from the building leading edge is important, and roof shapes with least amount of variability should be preferred for urban wind energy installation.

Another important factor in consideration to the power performance of a turbine is the fluctuations in power. Fig. 8(b) shows the standard deviation in power production normalized by maximum mean power extracted by the turbine at a certain position. Closer to the roof leading edge, all cases show similar values of normalized standard deviation in power of around 0.3, which in itself is a high number and can be attributed to high turbulence in the upstream boundary layer. Cube and Round cases initially show comparable values closer to the roof edge, where the difference between the two grows for $x/d > 1$. The Fence case, on the other hand, shows a significant increase in normalized standard deviation, with the values reaching as high as 1.29 at $x/d = 3$. In addition to the flow separation from the roof leading edge, the poor performance of the turbine on the back end of the roof in the Fence case can also be related to the additional blockage caused by the fence at the back end of the building.

To understand the effect of the turbine rotational speed on the power production, Fig. 9 shows the power production of the

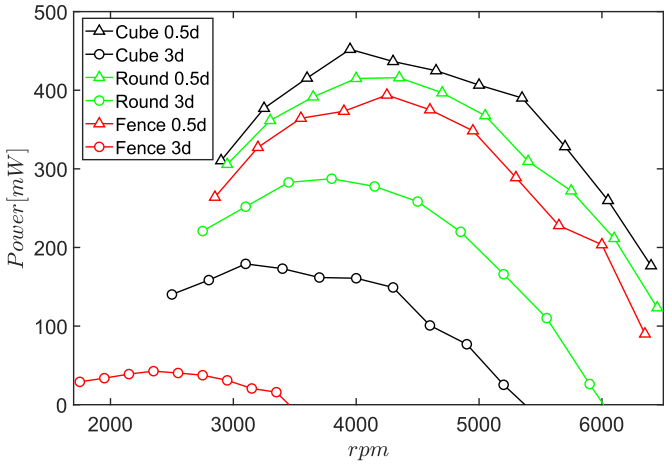

Fig. 9. Mean power produced by the turbine as a function of turbine rotational speed for different streamwise positions.

turbine at two different streamwise positions for different roof shapes. These positions correspond to the maximum and minimum values of P_{max} across the streamwise extent of the building, as observed in Fig. 8(a). The range of the turbine rotational speed differs in different cases to ensure that the tip speed ratio remains the same. Similar to the trend of power coefficient seen in Fig. 1 for flat terrain, the extracted power for a certain case first increases with the increase in rotor speed before reaching a maximum value beyond which, a decrease in power is observed with an increase in the rotational speed. The effect of roof shape is observed for the whole range of rotational speed, where the difference in power between different cases is smaller at $x/d = 0.5$, but grows significantly at $x/d = 3$.

To explain the variation in power production with the turbine position and roof edge shape, we plot the vertical profiles of averaged streamwise velocity and its standard deviation for several streamwise positions in Fig. 10. Power available for a turbine scales with the cube of velocity, therefore higher velocity across the rotor would mean that more power is available for the turbine. As can be seen in Fig. 10, at $x/d = 0.5$ the Cube and Round shape cases show similar velocity profiles, whereas the Fence case shows high shear

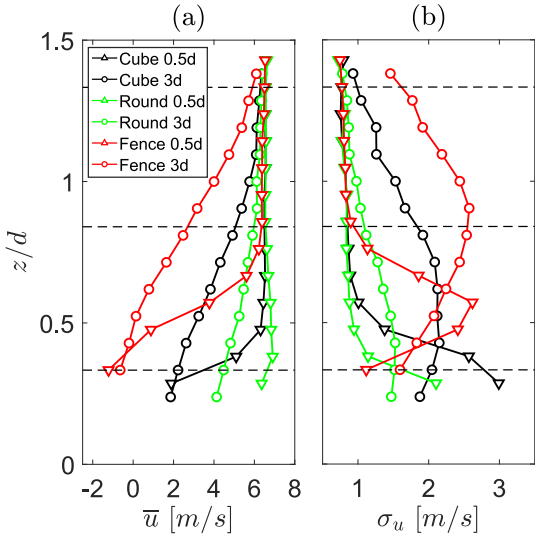

Fig. 10. (a) Vertical profiles of averaged streamwise velocity and (b) standard deviation of streamwise velocity across the rotor for different streamwise positions. The dashed horizontal lines trace the rotor bottom tip, hub and top tip locations.

in the bottom half of the rotor. For each case, this is the streamwise location where maximum velocity is observed across the rotor, thereby resulting in maximum power produced by the turbine. The relatively lower velocity encountered across the rotor at $x/d = 3$ results in the low power production obtained at this location, where the Fence case shows lowest values across the whole rotor compared to the other cases. The differences between the velocity profiles at 0.5 and 3 rotor diameters for each case appear to be consistent with the differences in the power production observed between these positions. For the fluctuations in power observed in Fig. 8(b), the standard deviation in the streamwise velocity profiles provides useful insights. Highest standard deviation values across the rotor, with a peak around the turbine hub height are observed for the Fence case at $x/d = 3$, which is consistent with the highest fluctuations in power observed at this location. The peak value of standard deviation at $x/d = 0.5$ is similar to that at $x/d = 3$ for the Fence case, although the location of peak is in the lower half of the rotor, with relatively smaller values in the upper half of the rotor, thereby resulting in lesser fluctuations in power. The Round case shows smaller standard deviation values compared to the other cases, which explains lower power fluctuations in this case. The Cube case shows standard deviation higher than the Round case, but smaller than the Fence one, resulting in power fluctuations more comparable to the Round case than the Fence one.

The dependency of the power produced by the turbine on its streamwise position, as well as on the roof edge shape is clearly shown. Building with curved roof edges is found to perform best and in a practical scenario, such building should be preferred for wind turbine siting. For the wake flow analysis in the following section, the turbine is placed at the streamwise position of $x/d = 0.5$, as it performs best in terms of power at this streamwise position. This is in accordance with how a turbine siting would be done in reality, where turbines are commonly placed at positions corresponding to the highest available resources.

3.3. Wake flow

We now investigate the wake of the turbine; specifically, we are interested in the comparison of the turbine wake for different roof edge shapes. Fig. 11 shows vertical profiles of the normalized averaged streamwise velocity in the turbine wake for different roof shapes. The profiles of normalized averaged streamwise velocity in the base flow are also included as a reference in this figure. The normalized averaged streamwise velocity in the wake is found to be highly dependent on the roof shape, where its magnitude is highest for the Round case and lowest for the Fence case. The symmetry of the velocity profile, especially on top of the building, is also observed to be affected by the roof shape, with relatively more symmetric profiles for the Round case. For the Cube and Fence cases, the profiles become asymmetric, with the Fence case showing highest asymmetry. Both the magnitude of the velocity and symmetry of the velocity profiles in the wake are consistent with the base flow velocity profiles, which showed least (highest) shear and highest (lowest) velocity for the Round (Fence) case. The Fence case is particularly interesting, as it shows negative velocities in the wake below the hub height on top of the building. This can be related to the relatively strong flow separation from the leading edge, as well as to the blockage and formation of a vortex in front of the back fence on the building. Behind the building, an enhanced expansion of the wake is observed, where the velocity differences between different cases follow the same trend as that on the building. Below the building height, the differences between the turbine wake and base flow increase with the increase in the distance, which could be associated with the downward trajectory of the turbine wake and its interaction with the building wake.

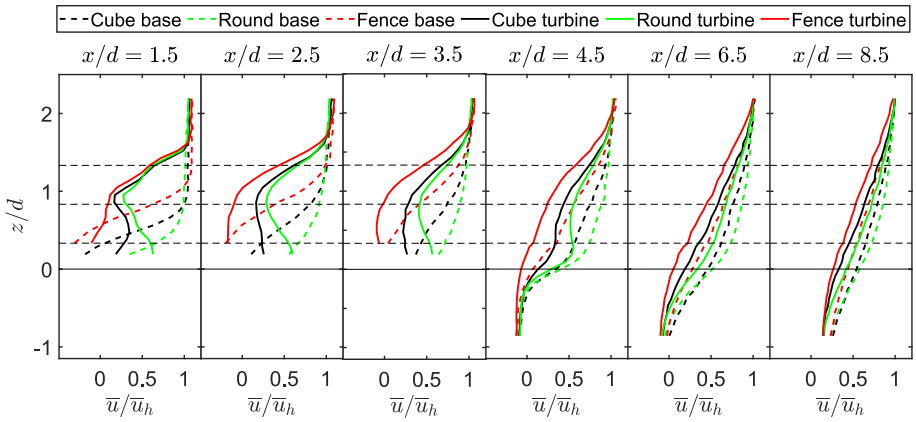

Fig. 11. Vertical profiles of the normalized averaged streamwise velocity in the turbine wake across the building. The base flow profiles are added for reference. The horizontal black solid line traces the height of the building, whereas the horizontal black dashed lines trace the prospective rotor bottom tip, hub and top tip locations.

To quantify the differences in the wake flow with respect to the base flow, we compute the streamwise velocity deficit $\Delta\overline{u} = \overline{u}_b - \overline{u}_w$, where $\overline{u}_b$ and $\overline{u}_w$ are the averaged streamwise velocities in the base and wake flow, respectively, at the same physical location. Fig. 12 shows the comparison of vertical profiles of the normalized averaged streamwise velocity deficit between different cases. Compared to the streamwise velocity profiles, the streamwise velocity deficit profiles show less difference between different cases. On top of the building the profiles appear to be fairly symmetric for all cases, whereas behind the building they show a relatively wider profile. A region of negative streamwise velocity deficit is observed close to the building leading edge for all cases. This is a result of flow speed up near the surface, as the turbine hinders the development of the separated flow from the building leading edge. To further characterize the streamwise wake velocity deficit, we plot the normalized maximum wake velocity deficit, the vertical position of the maximum wake velocity deficit and the normalized wake width as a function of downstream distance in Fig. 13.

The normalized maximum velocity deficit is used to characterize the recovery of the turbine wake center (Fig. 13 (a)). On top of the building, the normalized maximum velocity deficit is observed to be highest for the Fence case, with values decreasing for the Cube and Round case, respectively. As discussed by Dar & Porté-Agel [34], the normalized maximum velocity deficit is affected by the pressure gradient induced by the topography. Here the Fence case induces the highest pressure gradient on the wake, resulting in the highest value of the wake velocity deficit. The recovery of the velocity deficit is observed to be remarkably fast on top of the building, which could be related to the high turbulence intensity in the base flow. Behind the building, however, the recovery of the wake center slows down significantly for all cases. This can be related to the fact that, as the wake undergoes enhanced expansion due to the sudden absence of a surface, the recovery of the maximum velocity deficit has to slow down in order to conserve momentum.

To characterize the trajectory of the wake, we plot the normalized vertical position of the maximum velocity deficit (also called the wake center) in Fig. 13 (b). On top of the building, the wake center is observed to be above the hub height of the turbine for all cases, which can be related to the high vertical velocity experienced by the turbine in the base flow. The wake trajectory is also observed to be almost constant for all cases above the building. The Round and Cube cases show very similar wake trajectory above the building, whereas the Fence case shows a slightly higher location of the wake center compared to the rest. The presence of the fence above the building roof results in a high vertical velocity, which can explain the upward shift in the wake trajectory in this case. Behind the building the wake center moves down for all the cases, which indicates toward a downward movement of the turbine wake.

As the turbine wake moves downstream, it undergoes an expansion due to the shear layer developed from the rotor edge, which plays a role in the transport of energy in the wake from the outer flow. Wind turbine wakes are known to expand linearly as a function of downstream distance in the far wake in flat, as well as complex terrain [19,34]. As a result, the wake growth rate k in the

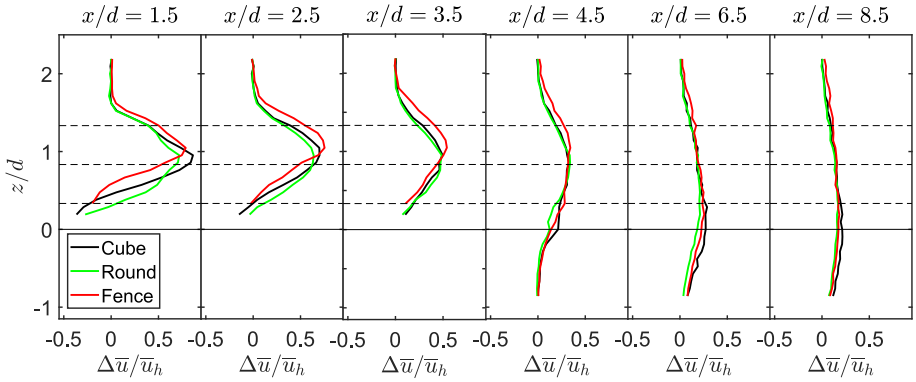

Fig. 12. Vertical profiles of the normalized averaged streamwise velocity deficit in the turbine wake across the building. The horizontal black solid line traces the height of the building, whereas the horizontal black dashed lines trace the prospective rotor bottom tip, hub and top tip locations.

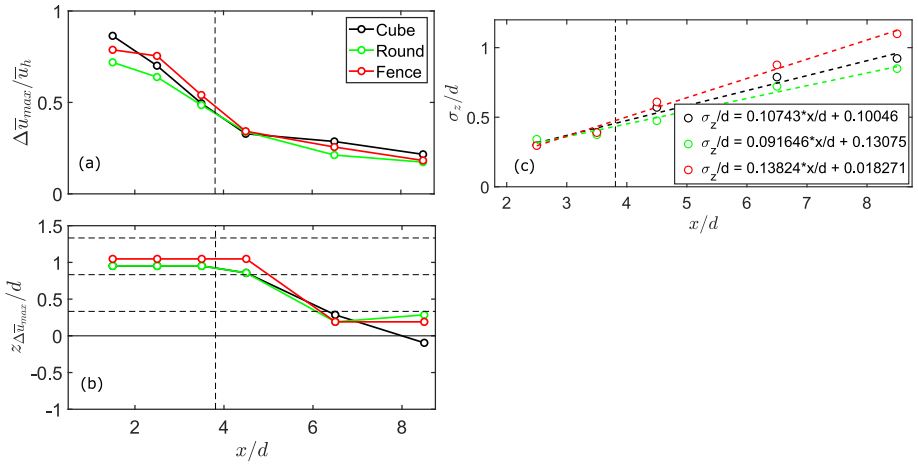

Fig. 13. (a) Maximum normalized velocity deficit, (b) vertical position of the maximum velocity deficit and (c) normalized standard deviation of the streamwise velocity deficit as a function of downstream distance. The horizontal black solid line in (b) traces the height of the building, whereas the black horizontal dashed lines trace the rotor bottom tip, hub and top tip locations. The vertical dashed black line marks the end of the building.

far wake can be estimated by the slope of a linear fit to the wake width such that:

$$\frac{\sigma_z}{d} = k\frac{x}{d} + \varepsilon, \tag{4}$$

where σ_z is the wake width estimated by the standard deviation of a Gaussian curve fitted to the vertical profile of the streamwise velocity deficit at each downstream position and ε is the initial wake width. Fig. 13 (c) shows the normalized wake width as a function of downstream distance, along with the linear fit according to equation (4) for the three cases. The wake growth rate is found to be highest for the Fence case, and decreases for the Cube and Round cases. It is also found to be significantly higher than the values typically reported in flat terrain (see, e.g. Ref. [42]) or those reported for a turbine sited on escarpments [34]. This is consistent with the relatively high streamwise turbulence intensity across the building compared to the flat terrain or escarpment studies. In addition, the sharp changes in the streamwise pressure gradient induced by the building could also play a role in different rate of expansion compared to flat terrain. The streamwise velocity deficit profiles are found to be Gaussian at $x/d = 2.5$ for all cases. This indicates that the near wake length is shorter than 2 rotor diameters, which is consistent with the high turbulence intensity in the base flow, as higher turbulence usually leads to a shorter near wake length.

Focusing on turbulence characteristics in the wake, we first plot the normalized averaged vertical momentum flux in Fig. 14. The vertical momentum flux is a key factor in determining the exchange of momentum between outer and wake flow, and plays a role in production of turbulence together with the mean flow shear. In the near wake ($x/d = 1.5$), all three cases show similar values of normalized averaged vertical momentum flux. However, in the far wake, the Fence case shows significantly higher values than the rest of the cases, with a peak around the rotor top tip height at $x/d = 3.5$. In previous studies on flat [36] and complex terrain [34], the vertical momentum flux is observed to be negative in the upper half of the rotor and positive in the lower half, especially for downstream distances shorter than 8 rotor diameters. In the current study, only the Round case depicts the behavior described above, whereas the Cube and Fence cases show predominantly a negative vertical momentum flux across the whole rotor, with relatively smaller values in the lower half of the rotor. Relatively high vertical momentum flux in the shear layer developed from the building leading edge in the base flow is believed to play a role in the above described behavior. The fact that the peak of the vertical momentum flux in the base flow on top of the building is located closer to the surface and found to be significantly higher than that in the wake flow helps explain the observed trend. Behind the building, the vertical momentum flux in the turbine wake is found to be comparable to that in the base flow, with slightly higher values in the turbine wake than the base flow.

The streamwise turbulence intensity in the turbine wake is shown in Fig. 15. Consistent with the vertical momentum flux, the streamwise turbulence intensity is observed to be highest in the Fence case, with values decreasing for the Cube and Round case. On top of the building, the streamwise turbulence intensity shows a peak around the rotor top tip height. Wu & Porté-Agel [43] performed a kinetic energy budget analysis to show that even though momentum fluxes are high across the whole rotor projected area, the peak in turbulence intensity at the rotor top tip height appears due to high mean flow shear around that height. A similar reasoning can be used here to explain the peak around the rotor top tip height. In addition, the peak value of streamwise turbulence intensity in the wake is observed to be smaller than that in the base flow. This will be discussed in detail below. Behind the building, the streamwise turbulence intensity profile flattens out, mainly because the mean flow shear becomes almost constant (see Fig. 11).

The streamwise turbulence intensity in the turbine wake is contributed by two sources: the one in the base flow and the one added or subtracted by the turbine. To quantify the streamwise turbulence intensity contributed by the turbine, we compute the added streamwise turbulence intensity I_{add}:

$$I_{add} = \begin{cases} +\sqrt{I_{u,w}^2 - I_{u,b}^2}, & I_{u,w} \geq I_{u,b}, \\ -\sqrt{I_{u,b}^2 - I_{u,w}^2}, & I_{u,w} < I_{u,b}, \end{cases}$$

where $I_{u,w}$ and $I_{u,b}$ are the streamwise turbulence intensities in the turbine wake and base flow, respectively. Fig. 16 shows the vertical profiles of the added streamwise turbulence intensity. The peak of the positive added streamwise turbulence intensity around the rotor top tip is found to be the same in all three cases. This indicates that the difference in the peak of streamwise turbulence intensity between different cases in the turbine wake comes from the

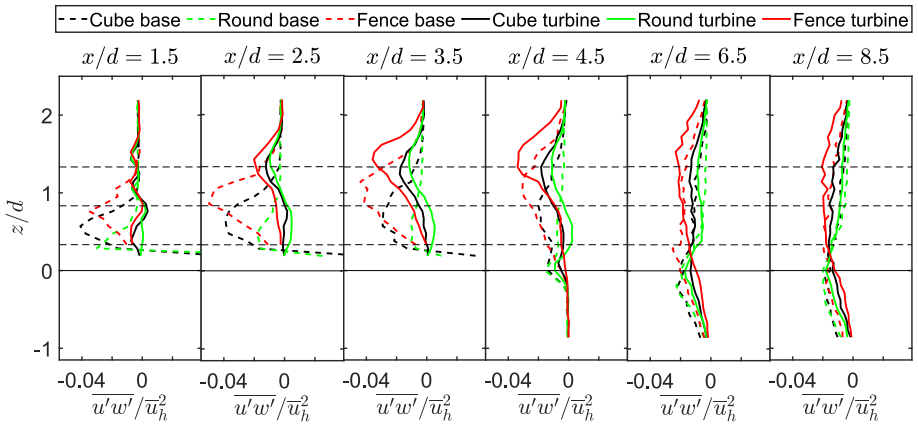

Fig. 14. Vertical profiles of the normalized averaged vertical momentum flux in the turbine wake across the building. The base flow profiles are added for reference. The horizontal black solid line traces the height of the building, whereas the horizontal black dashed lines trace the prospective rotor bottom tip, hub and top tip locations.

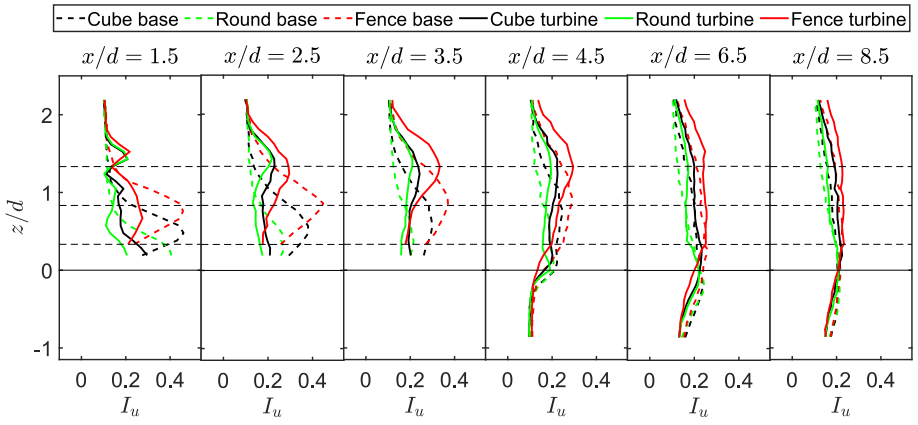

Fig. 15. Vertical profiles of the streamwise turbulence intensity in the turbine wake across the building. The base flow profiles are added for reference. The horizontal black solid line traces the height of the building, whereas the horizontal black dashed lines trace the prospective rotor bottom tip, hub and top tip locations.

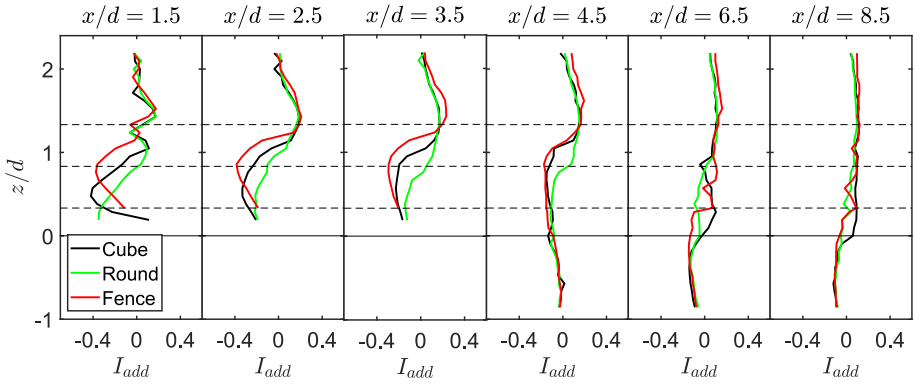

Fig. 16. Vertical profiles of the added streamwise turbulence intensity in the turbine wake across the building. The horizontal black solid line traces the height of the building, whereas the horizontal black dashed lines trace the prospective rotor bottom tip, hub and top tip locations.

difference in the base flow turbulence intensity, whereas the turbine contribution remains constant.

A region of negative added streamwise turbulence intensity above the building is observed in all cases. The negative added streamwise turbulence intensity means that the turbine suppresses turbulence in the wake compared to that in the base flow. Dar & Porté-Agel [34] explained that this negative added streamwise turbulence intensity appears because the turbine suppresses the development of the shear layer from the escarpment (in the current work, the building) leading edge in its wake. As the mean flow shear in the turbine wake close to the surface is lower than that in the base flow, the turbulence production is suppressed. While the positive added streamwise turbulence intensity is insensitive to the roof shape, the negative added streamwise turbulence intensity depends on the roof shape. The Fence case shows highest suppression of the streamwise turbulence intensity. In the Fence case,

apart from the region around the rotor top tip, the profile is predominantly negative, with the magnitude of the peak value higher than that for the positive added streamwise turbulence intensity. The peak position and magnitude of the negative added streamwise turbulence intensity decrease for the Cube case, which further decrease for the Round case. Behind the building, all three cases show similar profiles, with approximately constant values at $x/d \geq 6.5$.

4. Summary

In this study, we performed wind tunnel experiments on a roof-mounted horizontal-axis wind turbine placed in an urban environment. Of particular interest was the effect of roof edge shape on power performance and wake characteristics of a turbine sited on top of a tall cubic building. In addition, the effect of streamwise position of the turbine on its power performance was also investigated. The roof edge shapes were inspired from the ones observed in reality: a roof with sharp 90° edges (Cube case), a roof with slightly curved roof edges (Round case) and a roof with a solid boundary fence (Fence case). The modifications in the roof edge shapes could easily be deemed minor in a conventional resource assessment study, however, our results showed that such small modifications can significantly affect both the power performance and the wake of a turbine sited on top of the building.

The flow velocity, shear and streamwise turbulence intensity in the base flow were observed to be highly dependent on the roof edge shape. This was related to the growth of the shear layer due to flow separation from the building leading edge. This shear layer was found to be strongest in the Fence case, followed by the Cube and Round cases, respectively. As a result, the power available for a turbine was also dependent on the roof edge shape. All cases showed maximum mean power production at a streamwise distance of about half rotor diameter from the leading edge of the building. The Round case showed least variation in the maximum mean power production with the streamwise position and least amount of normalized standard deviation in power production. For the Cube case, maximum mean power production decreased after $x/d = 0.5$, where an increase in the normalized standard deviation was also observed. The Fence case showed highest drop in maximum mean power production, with values reaching approximately 10% at the back end of the building compared to those at the front end. The normalized standard deviation in power was also observed to be highest at the back end of the building for the Fence case, with values greater than 1 at $x/d \geq 2.5$.

For wake flow measurements, the turbine was placed at $x/d = 0.5$, as it corresponded to the position with highest power production. For all cases, the wake characteristics on top of the building and those behind the building showed significant differences, which were related to the sudden absence of a surface after the building edge. On top of the building, the normalized averaged streamwise velocity profiles in the wake showed differences between different cases, with higher velocity and relatively symmetric profiles for the Round case. The wake velocity was observed to be smaller and have more asymmetric profiles for the Cube and Fence cases, which was related to the separation induced by the leading edge in the base flow. The Fence case showed highest normalized streamwise velocity deficit above the building, with values decreasing for the Cube and Round case, respectively. The recovery of the wake center velocity deficit was found to be faster on top of the building, whereas it slowed down behind the building due to the sudden expansion of the wake. The wake growth rate was found to be highest in the Fence case, with values decreasing for the Cube and Round cases. The wake growth rate was also observed to be higher than the values typically reported in flat or complex terrain, which was associated with high base flow turbulence intensity across the building. The Fence case also showed relatively higher turbulence in the wake compared to the rest of the cases, whereas the turbulence added by the turbine was found to be the same around the rotor top tip height in all cases. The turbine also suppressed the turbulence production near the surface, as it suppressed the growth of the shear layer due to flow separation from the building leading edge. This negative added turbulence was found to be dependent on the case with highest magnitude in the Fence case and lowest in the Round case.

In conclusion, the sensitivity of both the power production and wake characteristics to the roof edge shape is clearly shown. Ideally, building shapes with least variation in power with position should be chosen to account for wind direction changes. The flow separation and shear layer development from the building edge are found to be the differentiating factor for the power and wake characteristics of a turbine. For the numerical modeling and resource assessment community, these results emphasize the importance of accurate building modeling, as seemingly minor differences in the roof edge shape can result in huge differences in the estimation of power production and wake effects of a roof mounted turbine.

Funding

This research was funded by the Swiss National Science Foundation (grant number: 200021_172538) and the Swiss Federal Office of Energy (grant number: SI/502135-01).

CRediT authorship contribution statement

Arslan Salim Dar: Conceptualization, Methodology, Investigation, Formal analysis, Writing – original draft, Supervision. **Guillem Armengol Barcos:** Conceptualization, Methodology, Investigation, Data curation, Formal analysis, Writing – review & editing. **Fernando Porté-Agel:** Conceptualization, Methodology, Supervision, Resources, Writing – review & editing, Funding acquisition.

Declaration of competing interest

The authors declare that they have no known competing financial interests or personal relationships that could have appeared to influence the work reported in this paper.

Nomenclature

C_p	Power coefficient
P	Mean power
Q	Shaft torque
Ω	Turbine rotational speed
ρ	Air density
A	Rotor swept area
C_T	Thrust coefficient
T	Thrust force
Re_d	Reynolds number based on turbine diameter
λ	Tip speed ratio
rpm	Revolutions per minute
x	Streamwise distance/coordinate
z	Vertical distance/coordinate
d	Turbine diameter
z_h	Turbine hub height
$z_{h,up}$	Projected height of turbine center on the building
d_0	Displacement height
z_0	Aerodynamic surface roughness
δ	Boundary layer height

n	Shear exponent
L	Length of square-base prism
h	Height of square-base prism
H	Height of cubic building
$\bar{u}$	Averaged streamwise velocity
$\bar{w}$	Averaged vertical velocity
$\bar{u}_h$	Averaged streamwise velocity at hub height
$\bar{u}_\infty$	Averaged free-stream velocity
u_*	Friction velocity
κ	von-Karman constant
I_u	Streamwise turbulence intensity
σ_u	Standard deviation in streamwise velocity
$\overline{u'w'}$	Averaged vertical momentum flux
$P_{\max}$	Maximum mean power
σ_P	Standard deviation in power
sl_c	Shear layer center
$\overline{\Delta u}$	Averaged streamwise velocity deficit
$\bar{u}_w$	Averaged streamwise velocity in the wake
$\bar{u}_b$	Averaged streamwise velocity in the base flow
Δu_{max}	Maximum streamwise velocity deficit
σ_z	Standard deviation in vertical profiles of streamwise velocity deficit
$z_{\overline{\Delta u}_{max}}$	Vertical position of maximum streamwise velocity deficit
k	Wake growth rate
ε	Initial wake width
I_{add}	Added streamwise turbulence intensity
$I_{u,w}$	Streamwise turbulence intensity in the wake
$I_{u,b}$	Streamwise turbulence intensity in the base flow

References

[1] United Nations Population Division, World Urbanization Prospects (No. 216), United Nations, Department of International Economic and Social Affairs, 2001.
[2] H. Ritchie, M. Roser, Urbanization. Our World in Data, 2018.
[3] U.N. Desa, Transforming Our World: the 2030 Agenda for Sustainable Development, 2016.
[4] A. Rezaeiha, H. Montazeri, B. Blocken, A framework for preliminary large-scale urban wind energy potential assessment: roof-mounted wind turbines, Energy Convers. Manag. 214 (2020), 112770.
[5] T. Stathopoulos, H. Alrawashdeh, A. Al-Quraan, B. Blocken, A. Dilimulati, M. Paraschivoiu, P. Pilay, Urban wind energy: some views on potential and challenges, J. Wind Eng. Ind. Aerod. 179 (2018) 146–157.
[6] D. Micallef, G. van Bussel, A review of urban wind energy research: aerodynamics and other challenges, Energies 11 (9) (2018) 2204.
[7] S.L. Walker, Building mounted wind turbines and their suitability for the urban scale—a review of methods of estimating urban wind resource, Energy Build. 43 (8) (2011) 1852–1862.
[8] B. Evans, J. Parks, K. Theobald, Urban wind power and the private sector: community benefits, social acceptance and public engagement, J. Environ. Plann. Manag. 54 (2) (2011) 227–244.
[9] N. Mithraratne, Roof-top wind turbines for microgeneration in urban houses in New Zealand, Energy Build. 41 (10) (2009) 1013–1018.
[10] D.R. Drew, J.F. Barlow, T.T. Cockerill, Estimating the potential yield of small wind turbines in urban areas: a case study for Greater London, UK, J. Wind Eng. Ind. Aerod. 115 (2013) 104–111.
[11] B. Grieser, Y. Sunak, R. Madlener, Economics of small wind turbines in urban settings: an empirical investigation for Germany, Renew. Energy 78 (2015) 334–350.
[12] M. Bayoumi, D. Fink, G. Hausladen, Extending the feasibility of high-rise façade augmented wind turbines, Energy Build. 60 (2013) 12–19.
[13] I. Abohela, N. Hamza, S. Dudek, Effect of roof shape, wind direction, building height and urban configuration on the energy yield and positioning of roof mounted wind turbines, Renew. Energy 50 (2013) 1106–1118.
[14] A. Al-Quraan, T. Stathopoulos, P. Pillay, Comparison of wind tunnel and on site measurements for urban wind energy estimation of potential yield, J. Wind Eng. Ind. Aerod. 158 (2016) 1–10.
[15] F.C. Emejeamara, A.S. Tomlin, A method for estimating the potential power available to building mounted wind turbines within turbulent urban air flows, Renew. Energy 153 (2020) 787–800.
[16] C.A. Ruiz, I. Kalkman, B. Blocken, Aerodynamic design optimization of ducted openings through high-rise buildings for wind energy harvesting, Build. Environ. (2021), 108028.
[17] S. Li, Y. Li, C. Yang, Q. Wang, B. Zhao, D. Li, R. Zhao, T. Ren, X. Zheng, Z. Gao, W. Xu, Experimental investigation of solidity and other characteristics on dual vertical axis wind turbines in an urban environment, Energy Convers. Manag. 229 (2021), 113689.
[18] S. Higgins, T. Stathopoulos, Application of artificial intelligence to urban wind energy, Build. Environ. 197 (2021), 107848.
[19] F. Porté-Agel, M. Bastankhah, S. Shamsoddin, Wind-turbine and wind-farm flows: a review, Boundary-Layer Meteorol. 174 (1) (2020) 1–59.
[20] R.J. Stevens, C. Meneveau, Flow structure and turbulence in wind farms, Annu. Rev. Fluid Mech. 49 (2017) 311–339.
[21] M. Hansen, Aerodynamics of Wind Turbines, Routledge, 2015.
[22] J.N. Sørensen, General Momentum Theory for Horizontal Axis Wind Turbines, Springer, 2016.
[23] M. Ge, S. Zhang, H. Meng, H. Ma, Study on interaction between the wind-turbine wake and the urban district model by large eddy simulation, Renew. Energy 157 (2020) 941–950.
[24] M. Ge, D.F. Gayme, C. Meneveau, Large-eddy simulation of wind turbines immersed in the wake of a cube-shaped building, Renew. Energy 163 (2021) 1063–1077.
[25] X. Fan, M. Ge, W. Tan, Q. Li, Impacts of coexisting buildings and trees on the performance of rooftop wind turbines: an idealized numerical study, Renew. Energy 177 (2021) 164–180.
[26] W. Xu, G. Li, X. Zheng, Y. Li, S. Li, C. Zhang, F. Wang, High-resolution numerical simulation of the performance of vertical axis wind turbines in urban area: Part I, wind turbines on the side of single building, Renew. Energy 177 (2021) 461–474.
[27] W. Xu, Y. Li, G. Li, S. Li, C. Zhang, F. Wang, High-resolution numerical simulation of the performance of vertical axis wind turbines in urban area: Part II, array of vertical axis wind turbines between buildings, Renew. Energy 176 (2021) 25–39.
[28] H.D. Nedjari, O. Guerri, M. Saighi, CFD wind turbines wake assessment in complex topography, Energy Convers. Manag. 138 (2017) 224–236.
[29] J. Dai, Y. Tan, W. Yang, L. Wen, X. Shen, Investigation of wind resource characteristics in mountain wind farm using multiple-unit SCADA data in Chenzhou: a case study, Energy Convers. Manag. 148 (2017) 378–393.
[30] W.C. Radünz, Y. Sakagami, R. Haas, A.P. Petry, J.C. Passos, M. Miqueletti, E. Dias, The variability of wind resources in complex terrain and its relationship with atmospheric stability, Energy Convers. Manag. 222 (2020), 113249.
[31] J. Lange, J. Mann, J. Berg, D. Parvu, R. Kilpatrick, A. Costache, J. Chowdhury, K. Siddiqui, H. Hangan, For wind turbines in complex terrain, the devil is in the detail, Environ. Res. Lett. 12 (9) (2017) 94020.
[32] G.W. Qian, T. Ishihara, Numerical study of wind turbine wakes over escarpments by a modified delayed detached eddy simulation, J. Wind Eng. Ind. Aerod. 191 (2019) 41–53.
[33] September A.S. Dar, F. Porté-Agel, Three-dimensional wind-turbine wake characterization via tomographic particle-image velocimetry, in: Journal of Physics: Conference Series, vol. 1618, IOP Publishing, 2020, p. 62045, 6.
[34] A.S. Dar, F. Porté-Agel, Wind-turbine wakes on escarpments: a wind-tunnel study, Renew. Energy 181 (2022) 1258–1275.
[35] M. Bastankhah, F. Porté-Agel, A new miniature wind turbine for wind tunnel experiments. Part I: design and performance, Energies 10 (7) (2017) 908.
[36] M. Bastankhah, F. Porté-Agel, A new miniature wind turbine for wind tunnel experiments. Part ii: wake structure and flow dynamics, Energies 10 (7) (2017) 923.
[37] M. Bastankhah, F. Porté-Agel, Experimental and theoretical study of wind turbine wakes in yawed conditions, J. Fluid Mech. 806 (2016) 506–541.
[38] I.P. Castro, H. Cheng, R. Reynolds, Turbulence over urban-type roughness: deductions from wind-tunnel measurements, Boundary-Layer Meteorol. 118 (1) (2006) 109–131.
[39] W.C. Cheng, F. Porté-Agel, Adjustment of turbulent boundary-layer flow to idealized urban surfaces: a large-eddy simulation study, Boundary-Layer Meteorol. 155 (2) (2015) 249–270.
[40] R.B. Stull, An Introduction to Boundary Layer Meteorology, vol. 13, Springer Science, 2012.
[41] M. Kiya, K. Sasaki, Structure of a turbulent separation bubble, J. Fluid Mech. 137 (1983) 83–113.
[42] W.C. Cheng, F. Porté-Agel, A simple physically-based model for wind-turbine wake growth in a turbulent boundary layer, Boundary-Layer Meteorol. 169 (1) (2018) 1–10.
[43] Y.T. Wu, F. Porté-Agel, Atmospheric turbulence effects on wind-turbine wakes: an LES study, Energies 5 (12) (2012) 5340–5362.